

# Endocytosis of a Glycosylphosphatidylinositol-anchored Protein via Clathrin-coated Vesicles, Sorting by Default in Endosomes, and Exocytosis via RAB11-positive Carriers<sup>□</sup>

Christoph G. Grünfelder,\* Markus Engstler,† Frank Weise,\* Heinz Schwarz,‡  
York-Dieter Stierhof,§ Gareth W. Morgan,|| Mark C. Field,|| and Peter Overath\*¶

\*Max-Planck-Institut für Biologie, Abteilung Membranbiochemie, D-72076 Tübingen, Germany; †Ludwigs-Maximilians-Universität München, Department Biologie I, Bereich Genetik, D-80638 München, Germany; ‡Max-Planck-Institut für Entwicklungsbiologie, D-72076 Tübingen, Germany; §Zentrum für Molekularbiologie der Pflanzen, Universität Tübingen, D-72076 Tübingen, Germany; and ||Wellcome Trust Laboratories for Molecular Parasitology, Imperial College London, Department of Biological Sciences and Centre for Molecular Microbiology and Infection, London, SW7 2AY, United Kingdom

Submitted October 10, 2002; Revised December 3, 2002; Accepted 2003  
Monitoring Editor: Jennifer-Lippincott-Schwartz

Recently, proteins linked to glycosylphosphatidylinositol (GPI) residues have received considerable attention both for their association with lipid microdomains and for their specific transport between cellular membranes. Basic features of trafficking of GPI-anchored proteins or glycolipids may be explored in flagellated protozoan parasites, which offer the advantage that their surface is dominated by these components. In *Trypanosoma brucei*, the GPI-anchored variant surface glycoprotein (VSG) is efficiently sorted at multiple intracellular levels, leading to a 50-fold higher membrane concentration at the cell surface compared with the endoplasmic reticulum. We have studied the membrane and VSG flow at an invagination of the plasma membrane, the flagellar pocket, the sole region for endo- and exocytosis in this organism. VSG enters trypanosomes in large clathrin-coated vesicles (135 nm in diameter), which deliver their cargo to endosomes. In the lumen of cisternal endosomes, VSG is concentrated by default, because a distinct class of small clathrin-coated vesicles (50–60 nm in diameter) budding from the cisternae is depleted in VSG. TbRAB11-positive cisternal endosomes, containing VSG, fragment by an unknown process giving rise to intensely TbRAB11- as well as VSG-positive, disk-like carriers (154 nm in diameter, 34 nm in thickness), which are shown to fuse with the flagellar pocket membrane, thereby recycling VSG back to the cell surface.

## INTRODUCTION

To a large extent, the specific composition of cellular membranes is achieved and maintained by the selective transport of integral membrane components by way of vesicular car-

riers, which shuttle between different cellular compartments. Paradigmatic are two positive sorting mechanisms: First, trans-membrane proteins in a donor membrane can be specifically incorporated into coated membrane domains, which bud off as transport vesicles and fuse with the target membrane (Kirchhausen, 2000); and second, certain lipids or lipid-anchored proteins are proposed to form liquid-ordered microdomains in the fluid-disordered bulk phase of a membrane and these domains are then considered to be selectively incorporated into carrier vesicles (Simons and van Meer, 1988; Simons and Ikonen, 1997; Brown and London, 2000). Positive selection implies concurrent negative selection or sorting by default, because the concentration of components excluded from coated vesicles or lipid microdomains increases as positively selected proteins and lipids are removed. The remaining membrane can thus be a source for vesicular carriers specifically enriched in unselected components.

Article published online ahead of print. Mol. Biol. Cell 10.1091/mbc.E02-10-0640. Article and publication date are at [www.molbiolcell.org/cgi/doi/10.1091/mbc.E02-10-0640](http://www.molbiolcell.org/cgi/doi/10.1091/mbc.E02-10-0640).

<sup>□</sup> Online version of this article contains video material. Online version of this article is available at [www.molbiolcell.org](http://www.molbiolcell.org).

<sup>¶</sup> Corresponding author. E-mail address: [peter.overath@tuebingen.mpg.de](mailto:peter.overath@tuebingen.mpg.de).

Abbreviations used: GPI, glycosylphosphatidylinositol; VSG, variant surface glycoprotein; AMCA, 7-amino-4-methylcoumarin; FP, flagellar pocket; CCV, clathrin-coated vesicle; EC, endosomal cisterna; EXC, exocytic carrier vesicle; PAG, protein A gold complex.

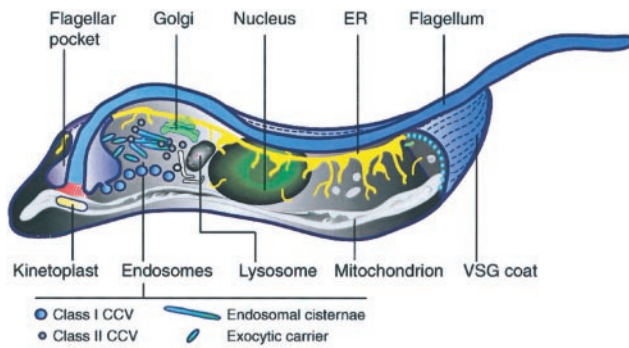


**Figure 1.** Schematic drawing of the ultrastructure of *T. brucei*. The figure presents a simplified version of the endocytic compartment comprising two classes of clathrin-coated vesicles and TbRAB11-positive structures involved in recycling of VSG. The white cisternae close to the lysosome represent a hypothetical, late endosomal compartment, which may be the target for class II clathrin-coated vesicles. Structures corresponding to early endosomes are not depicted because they have not yet been defined on the ultrastructural level.

We are interested in the cellular sorting of glycosylphosphatidylinositol (GPI)-anchored proteins, a class of cell surface proteins thought to occur in all eukaryotic cells, but studied mainly in mammalian cells, yeast, and kinetoplastid protozoa (McConville and Ferguson, 1993; Ferguson, 1999; Chatterjee and Mayor, 2001). The phosphatidylinositol residue confers on these proteins properties of “big lipids,” whereas the protein moiety allows for their ready detection by immunochemical techniques and, in some cases, by their enzymatic or ligand-binding properties. Therefore, these proteins have become popular for studies on cellular sorting, and depending on the cell type and the membrane compartments investigated, both positive and negative sorting scenarios have been proposed (Bretscher *et al.*, 1980; Bamezai *et al.*, 1992; Keller *et al.*, 1992; Simons and Ikonen, 1997; Harder *et al.*, 1998; Muñoz *et al.*, 2001; Sabharanjak *et al.*, 2002).

We have chosen the mammalian stage of the parasitic protozoan *Trypanosoma brucei* (see Figure 1 for relevant ultrastructural features of the organism), as a model for the sorting of GPI-anchored proteins for three reasons. First, this and related flagellates abundantly express GPI-anchored proteins. *T. brucei* is covered by a dense coat of the GPI-anchored variant surface glycoprotein (VSG), which comprises 10% of the total cellular protein (Overath *et al.*, 1994; Cross, 1996). Sorting is effective, because the concentration of VSG at the cell surface is 50 times higher than in the endoplasmic reticulum (ER) (Grünfelder *et al.*, 2002), where the protein is synthesized and the lipid anchor is attached. The concentration in membranes of the Golgi complex and of endosomes is 2.7 and 10.8 times higher than in membranes of the ER, respectively. Thus, the ratio of the VSG concentration at the cell surface to the average concentration on endosomal membranes seems to be 4.7. The second reason for using *T. brucei* is the highly compact and polarized arrangement of its structures involved in endo- and exocytosis. Macromolecular nutrient uptake as well as secretion is restricted to the flagellar pocket membrane, an invagination of the plasma membrane surrounding the emerging flagellum at the posterior end of the cell. Endosomes are exclusively located between the flagellar pocket and the nucleus

forming a prominent and in part continuous system of cisternal/tubulovesicular structures. In addition, this region harbors the single Golgi apparatus and the lysosome(s) (Overath *et al.*, 1997; Field *et al.*, 2000; Weise *et al.*, 2000; Landfear and Ignatushchenko, 2001; McConville *et al.*, 2002b). Third, the equivalent of the membrane area of the flagellar pocket is internalized every 2 min (Coppens *et al.*, 1987). This observation suggests that VSG is rapidly endocytosed and recycled (Seyfang *et al.*, 1990) and implies effective sorting in the endosomal system.

In this study, we focus on membrane structures involved in uptake and recycling of VSG in *T. brucei*. We show that VSG enters trypanosomes at the flagellar pocket in clathrin-coated vesicles and then associates with endosomes. VSG seems to be concentrated by default in cisternal endosomes by budding of a distinct class of clathrin-coated pits (CCPs) and vesicles, which are depleted in VSG. The cisternal endosomes give rise to VSG-rich, TbRAB11-positive exocytic carriers, which fuse with the flagellar pocket membrane. The results are discussed in comparison to sorting and membrane recycling of GPI-anchored proteins in mammalian cells, in which exocytic carriers recycling from endosomes to the plasma membrane have so far not been characterized (Sönnichsen *et al.*, 2000).

## MATERIALS AND METHODS

### Immunofluorescence

Bloodstream stage *Trypanosoma brucei* (strain MITat 1.2) were cultivated in HMI-9 + 10% fetal bovine serum, at 37°C in an atmosphere of 5% CO<sub>2</sub> in air. Cells were harvested at a density of 8 × 10<sup>5</sup> cells/ml by centrifugation at 1400 × g and 4°C for 10 min. After three washes with ice-cold trypanosome dilution buffer (TDB; 5 mM KCl, 80 mM NaCl, 1 mM MgSO<sub>4</sub>, 20 mM Na<sub>2</sub>HPO<sub>4</sub>, 2 mM NaH<sub>2</sub>PO<sub>4</sub>, 20 mM glucose, pH 7.4), the cell density was adjusted to 1 × 10<sup>8</sup> cells/ml and incubation with 1 mM sulfo-NHS-SS-biotin, 1 mM 7-amino-4-methylcoumarin (AMCA)-sulfo-NHS (both from Pierce Chemical, Rockford, IL) was performed for 10 min on ice in the dark. The reaction was stopped by the addition of 10 mM Tris-HCl, pH 8.5. After three washes with 2 ml of ice-cold TDB, the cell suspension was adjusted to a density of 4 × 10<sup>8</sup> cells/ml. Aliquots of 50 μl were added to 450 μl of prewarmed (37°C) HMI-9 and endocytosis was allowed for 3 min, followed by two washes with ice-cold TDB. Sulfo-NHS-SS-biotin was cleaved from the cell surface by 15 min of incubation on ice with 60% HMI-9, 10% fetal calf serum, 50 mM glutathione, pH 9.0. After two final washings with TDB, cells were fixed with 4% paraformaldehyde in phosphate-buffered saline (PBS) for 24 h at 4°C. Throughout the procedure, the cell viability was monitored by microscopy. Permeabilization of trypanosomes was achieved by 15-min incubation in 500 μl of 0.1 M Na<sub>2</sub>HPO<sub>4</sub>/1 M glycine, pH 7.2, followed by 5-min incubation in 1 ml of 0.05 M Na<sub>2</sub>HPO<sub>4</sub>/0.5 M glycine/0.1% Triton X-100, pH 7.2. Biotinylated, endocytosed VSG was detected with Alexa Fluor 594-conjugated streptavidin (10 μg/ml; Molecular Probes). For immunodetection of TbRAB11A (Jeffries *et al.*, 2001) and clathrin heavy chain (Morgan *et al.*, 2001), respectively, affinity-purified rabbit antibodies diluted 1:200 in PBS/1% bovine serum albumin were used. As secondary reagent Alexa Fluor 488-conjugated goat anti rabbit antibody (1:2000; Molecular Probes) was used.

Image acquisition was performed with a motorized Axiophot2 widefield microscope equipped with a 63×/1.4 numerical aperture oil DIC objective (both from Carl Zeiss, Thornwood, NY), a 2.5× optovar, and the CoolSnap HQ cooled (−30°C) charge-coupled device camera (Sony ICX285 interline, progressive-scan charge-coupled device). For acquisition of three-dimensional (3D)-images, a

PiFoc objective z-stepper was driven by the piezo-amplifier E662 LVPZT (Physik Instrumente, Karlsruhe, Germany). The microscopic setup was integrated and controlled using the scripting features of the IPLab for Macintosh software (version 3.5; Scanalytics, Fairfax, VA; for details, see <http://www.scanalytics.com/>). 3D images were acquired using the optimal sampling density derived from the optical setup and the respective fluorophor (z-step size  $\geq 50 \times 100$  nm). The point spread function of the microscope was measured using fluorescent 0.17- $\mu$ m microspheres (PS-Speck microscope point source kit; Molecular Probes). After image acquisition, the raw data were exported to the Huygens System software (version 2.1.8; Scientific Volume Imaging, B.V., Hilversum, The Netherlands; for details, see <http://www.svi.nl/>), and digital deconvolution was performed using the "maximum likelihood estimation" algorithm (>80 iterations). The restored image data set was visualized and analyzed with the Imaris software package, featuring the Full 3D and Surpass modules (version 3.1 for IRIX; Bitplane AG, Zurich, Switzerland (for details, see <http://www.bitplane.ch/products/Imaris/> and <http://www.bitplane.ch/products/ImarisSurpass/>). For animated presentation of 3D data, AMCA-stained cell surfaces were processed using the nonlinear morphological gradient filter implemented in the IPLab software. In this way a  $3 \times 3$  eroded version of the (blue) AMCA channel was created and merged with the nonprocessed red and green channels, allowing visualization through the cell surface of endocytosed VSG and TbRAB11 or clathrin heavy chain, respectively. Colocalization analysis of multichannel 3D data series was performed with the colocalization software (version 1.0 for IRIX; Bitplane AG; for details, see <http://www.bitplane.ch/products/colocalization/>).

### Immunoelectron Microscopy

Logarithmically growing trypanosomes of variant MITat 1.2 were either cryoimmobilized by high-pressure freezing as described previously (Grünfelder *et al.*, 2002) or chemically fixed for Tokuyasu cryosectioning. Cryo-fixed cells were freeze substituted in 0.5% glutaraldehyde + 0.5% osmium tetroxide ( $\text{OsO}_4$ ) in acetone from  $-90$  to  $-40^\circ\text{C}$  for 39 h (Figure 3A) or in 0.5%  $\text{OsO}_4$  in acetone from  $-90^\circ\text{C}$  to  $-40^\circ\text{C}$  for 36 h, followed by 0.25%  $\text{OsO}_4$  and 0.25% gallic acid in acetone for 30 h at  $-40^\circ\text{C}$  (Figure 3D). After washing with acetone, cells were embedded in Epon.

For cryosectioning, chemical fixation was performed in suspension for 3–5 min at room temperature, followed by 1.5–2 h on ice by using final concentrations of 4% formaldehyde in 0.1 M HEPES (pH 7.2) or 2% formaldehyde in 0.1 M HEPES supplemented with 0.05% glutaraldehyde. After fixation, cells were centrifuged, embedded in 1 or 2% low melting temperature agarose (SeaPlaque, Rockland, ME) in PBS, cut into small blocks, washed twice in PBS, and infiltrated with 20% polyvinylpyrrolidone/1.8 M sucrose in 0.1 M  $\text{Na}_2\text{HPO}_4$ . Specimen blocks were mounted on copper stubs, frozen in liquid nitrogen and trimmed and sectioned (at 60–70 nm) with a Leica Ultracut S/FCS cryo-ultramicrotome. The grids with the thawed cryosections were floated on ice cold PBS for storage before immunolabeling.

Immunolabeling of ultrathin Epon- and cryosections was performed according to standard protocols (Stierhof *et al.*, 1999). The following antibodies were used: rabbit anti-VSG MITat 1.2 antiserum (1:70; Grünfelder *et al.*, 2002), rabbit antibodies against *T. brucei* clathrin heavy chain (1:50), TbRAB11A (1:70), and biotin (affinity purified; 1:100; Loxo, Dossenheim, Germany). In single labeling, the primary antibodies were detected by 6 or 15 nm Protein A gold complexes (PAG-6 and PAG-15). For double labeling (Figures 3E, inset; 5, D–F), the first antibody was generally detected by PAG-10 or PAG-6; after a block with a rabbit normal IgG (1:400), the second antibody was detected by PAG-10 or PAG-15. In one case (Figure 3 E, inset), clathrin was first labeled with rabbit anti-TbCLH antibodies and PAG-6, whereas VSG was subsequently detected using biotinylated rabbit anti-VSG IgG followed by a monoclonal mouse anti-biotin antibody (1:100; Vector Laboratories, Burlingame,

CA) and goat anti-mouse IgG-18-nm gold conjugates (1:20; Jackson Immunoresearch Laboratories, West Grove, PA). After labeling, the cryosections were embedded in 1.4% methylcellulose, 0.3% uranyl acetate. Sections were analyzed in Philips CM10 and Philips 201 electron microscopes at 60 kV. Images were reproduced on baryt papers (final magnification, 80- to 100,000-fold), scanned at 300 dpi resolution, and digitally arranged to the plates by using the Color Photopaint program, version 10.

## RESULTS

We previously concluded from an analysis of the steady-state distribution of VSG in the mammalian stage of *T. brucei* that sorting of this protein occurs in multiple intracellular steps (Grünfelder *et al.*, 2002). From these steps, the VSG membrane concentration gradient of approximately 5 between the cell surface and an averaged estimate for endosomes seemed to be most readily accessible for further analysis. Using recently described, specific antibodies against the clathrin heavy chain and the small GTPase TbRAB11 (Morgan *et al.*, 2001, 2002a,b; Jeffries *et al.*, 2001), we have investigated endocytic and recycling membrane structures, which are involved in VSG trafficking from and to the flagellar pocket.

### Distribution of Clathrin and Endocytosed VSG

An overview of the intracellular distribution of clathrin in comparison with endosomal VSG was obtained by 3D immunofluorescence analysis. The cell surface was first double-labeled in the cold with cleavable sulfo-succinimidyl-2-(biotinamido)-ethyl-1,3-dithiopropionate (sulfo-NHS-SS-biotin) and noncleavable sulfo-succinimidyl-7-amino-4-methylcoumarin-3-acetic acid (AMCA-sulfo-NHS). After endocytosis to steady state (3 min at  $37^\circ\text{C}$ ; unpublished data), surface-associated biotin was removed by incubation with glutathione. Although AMCA-labeled VSG was endocytosed with the same kinetics as biotinylated VSG as shown by immunoelectron microscopy by using anti-AMCA antibodies (our unpublished data), the AMCA fluorescence was quantitatively quenched within the endocytic compartment. This fortuitous observation allowed us to visualize VSG on the cell surface, including the flagellar pocket membrane, as blue AMCA fluorescence, whereas endocytosed biotinylated VSG was detected through the red fluorescence of Alexa Fluor 594 conjugated to streptavidin. In combination with immunodetection of the clathrin heavy chain and Alexa Fluor 488-conjugated secondary antibodies, we were able to reconstruct a multichannel, three-dimensional distribution map of endosomal VSG- and clathrin-containing structures. Digitally deconvolved 3D data were analyzed using (animated) maximum intensity projection (Figure 2A), volume rendering (transparency blending) (Figure 2B), and shadow projection (Figure 2C; see legend for the advantages of the different visualization techniques).

As expected, endocytosed VSG filled part of the cellular space between the flagellar pocket and the nucleus (Figure 2A, labeled FP and N). The overall VSG distribution within this area, however, did not look diffuse, but formed a coherent compartment with sharp borders. In addition, clathrin-containing structures colocalizing with endocytosed VSG were found in distinct parts of the endocytic compartment. As shown in Figure 2B and C, clathrin was not only associ-

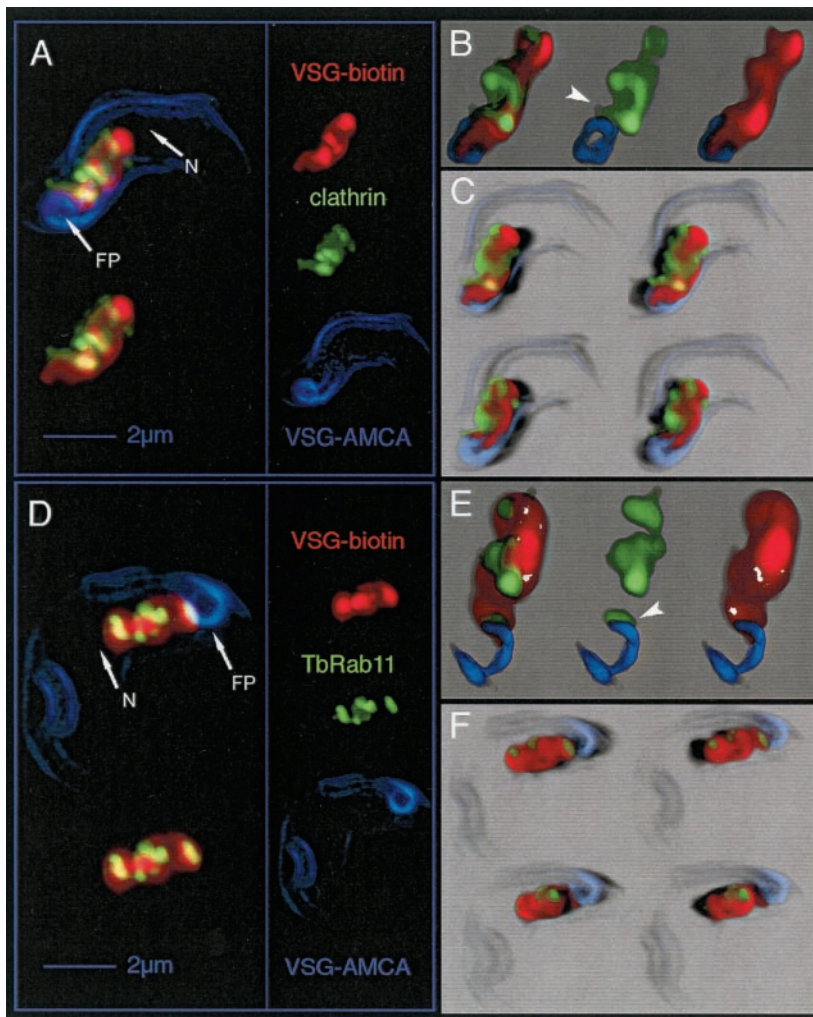


**Figure 2.** Analysis of the distribution of clathrin, TbRAB11, and endocytosed VSG in *T. brucei* by 3D image processing. The different fluorescence channels of deconvolved 3D images reduced in size to 66% are designated on the right in A and D: red, endocytosed biotin-labeled VSG; green, clathrin or TbRAB11; and blue, AMCA-labeled VSG located at cell surface. Three different visualization methods were applied to illustrate the 3D image information. (A and D) Maximum intensity projection (MIP) is a volume rendering technique that determines at each pixel the highest data value encountered along the corresponding viewing ray. The overall VSG distribution within the area between the FP and the nucleus (N) has a structured appearance with sharp borders. Both clathrin (A) and TbRAB11 (D) localize to distinct parts within this region. The upper left images represent the projection of all three fluorescence channels, whereas in the lower left images AMCA fluorescence has been omitted. 3D-animations of the MIP images shown herein, which allow a better navigation, can be found in the supplementary material to this article. (B and E) In addition to MIP, a volume-rendering technique uses the transparency information of the 3D data set to blend all values along the viewing direction (transparency blending). This offers the possibility to display also weak or fuzzy structures. Transparency blending reveals that clathrin and TbRAB11 are in fact localized to distinct sub-compartments of the endocytic system. In addition, a significant amount of the clathrin signal can be visualized outside of the VSG-containing structure. The juxtaposition of clathrin or TbRAB11 with respect to VSG at the flagellar pocket membrane is indicated by arrow heads. (C and F) Shadow projection is a ray-tracing technique that uses artificial light to illuminate structures. A viewing ray is sent through the volume image and, using the principle of the simulated fluorescence process, it is evaluated, which voxel is visible to what degree. This allows documentation of the spatial distribution of clathrin (C) and

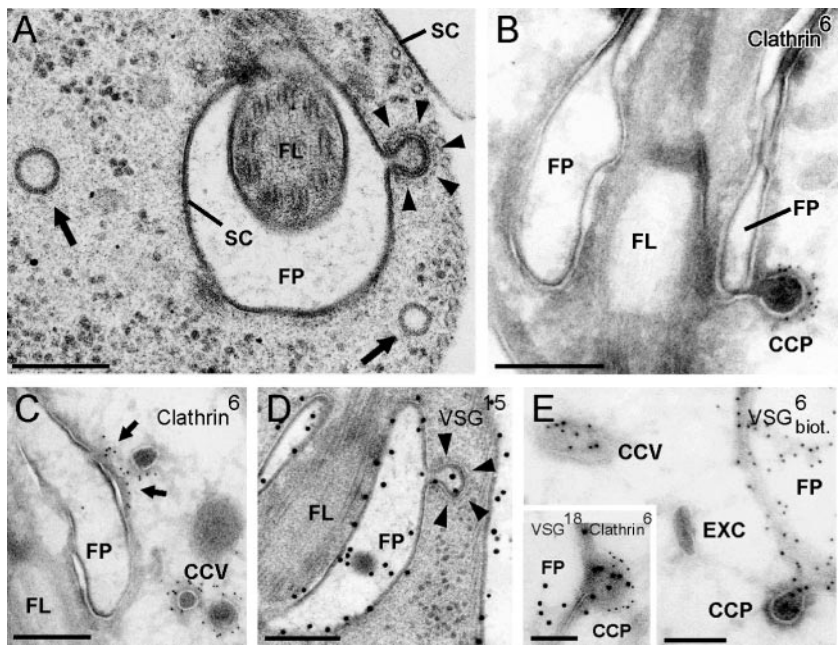
TbRAB11 (F) with respect to endocytosed VSG. Light directions and points of view were altered to allow visualization of cells from different sides (top, view from above; bottom, view from below). A significant amount of clathrin locates to the periphery of VSG-containing endosomes (C), whereas TbRAB11-positive structures seem embedded within the endocytic compartment (F).

ated with VSG-positive structures close to the flagellar pocket, but was also detectable in areas distant from the site of endocytosis. Volume-rendering (Figure 2B) and shadow projections (Figure 2C) indicated that a significant amount of clathrin was located at the periphery of the endocytic compartment. In quantitative terms,  $42.7 \pm 3.2\%$  of the endocytosed VSG colocalized with clathrin and  $65.8 \pm 4.3\%$  of clathrin colocalized with VSG ( $n = 15$ ), implying that a significant fraction of clathrin-associated structures did not carry VSG. The fidelity of our method was validated by documenting the complete absence of a colocalization signal between 1) clathrin and AMCA-conjugated VSG located on the cell surface, and 2) clathrin and specific markers for the ER and the lysosome (our unpublished data). The further characterization of the relationship of the two proteins in membrane trafficking required the resolution of the electron microscope.

### Endocytosis of VSG by Clathrin-coated Vesicles

For optimal ultrastructural preservation, trypanosomes were subjected to high-pressure freezing and freeze-substitution followed by Epon embedding. The electron micrographs shown in Figure 3, A and D, clearly document the VSG coat on the cell surface, on the membrane facing the flagellar pocket as well as the inner aspect of coated pits (arrowheads) and vesicles (arrows; average diameter,  $\sim 135$  nm). On all of these structures, 1) the fine-structural appearance, 2) the electron density, and 3) the thickness of the coat, as determined by a quantitative evaluation of perpendicularly sectioned membrane profiles, were very similar. All subsequent experiments were performed with cryosections. Figure 3, B, C, and E, shows that the electron-dense layer on the cytoplasmic side of coated pits and vesicles could be strongly labeled by anti-clathrin antibodies. Figure 3E depicts a flagellar pocket from cells surface-biotinylated at  $0^\circ\text{C}$

**Figure 3.** Endocytosis of VSG by clathrin-coated vesicles. (A) Section of a high-pressure frozen, freeze-substituted and Epon-embedded cell showing the FP and flagellum (FL). A clathrin-coated pit (coat marked by arrow heads) pinches off the flagellar pocket membrane and two endocytic vesicles (arrows), which have already lost their clathrin coat, can be seen in the cytoplasm. The VSG surface coat (SC) lines the flagellar pocket membrane and the inner face of coated pits and endocytic vesicles. (B and C) Cryosections labeled with anti-clathrin antibodies and PAG-6. Clathrin covers coated pits (CCP in B) and vesicles (CCV in C); a new coated pit forms at the flagellar pocket membrane in C (arrows). (D) Epon-section prepared as for A was labeled with anti-VSG antibodies and PAG-15. VSG enters a coated pit (arrow heads). (E) Cryosection labeled with rabbit anti-biotin antibodies and PAG-6. Cells were biotinylated at 0°C and then warmed to 26°C for 5 s to initiate endocytosis. Biotinylated VSG ( $VSG_{\text{biot}}$ ) enters a clathrin-coated pit and is present in a coated vesicle but the EXC is not labeled. The inset shows a coated pit double labeled for VSG with biotinylated anti-VSG antibodies (PAG-18) and clathrin (PAG-6; for further details, see MATERIALS AND METHODS). Bars (A–D), 250 nm; E, 125 nm.



and briefly heated to 26°C to allow endocytosis. Biotinylated VSG was clearly present in CCPs (Figure 3E, inset) and a pinched-off vesicle (CCV) but not in the exocytic carrier vesicle (EXC; see below). Therefore, these experiments prove that the extensively documented spiny coat on the cytoplasmic side of endocytic vesicles of *T. brucei* (Vickermann, 1969; Langreth and Balber, 1975; Webster and Grab, 1988) is indeed composed of clathrin as previously suggested (Webster and Shapiro, 1990; Morgan *et al.*, 2001). Based on criteria listed above, the VSG coat included in these vesicles is indistinguishable from that at the flagellar pocket membrane. We designate these vesicles as class I clathrin-coated vesicles.

On the average, sections through the flagellar pocket region showed three to four profiles of class I coated pits and vesicles. The abundance of these structures reflects the high rate of endocytosis in this organism. Preliminary experiments suggest that the endocytosed, biotinylated VSG is first delivered to cisternal structures located near the lysosome/nucleus and then moves via endosomes back to the flagellar pocket (Engstler and Grünfelder, unpublished data).

### Clathrin-coated Vesicles Depleted in VSG Bud from Endosomes

Endosome-associated clathrin, was first described in mammalian cells by Killish *et al.* (1992) and later in more detail by Stoorvogel *et al.* (1996). In their recent study, Morgan *et al.* (2001) showed by cryoimmunogold electron microscopy that clathrin immunoreactivity is widely distributed among membrane structures in the posterior region of *T. brucei* in agreement with the fluorescence microscopic analysis (Figure 2). Herein, we present the relationship between endosome-associated clathrin and VSG.

On the electron microscopic level, the endocytic compartment of *T. brucei* consists of a prominent system of narrow,

sheet-like cisternae (EC, for endocytic cisterna;  $30.7 \pm 0.3$  nm in thickness), which in cross sections, have an extended (Figure 4 A), or more rarely, circular shape (Figure 6, A and D, circular endosomal cisterna; cEC). The cisternae contain biotinylated VSG taken up by endocytosis from the cell surface (Overath *et al.*, 1994; our unpublished data). A common feature of endosomal cisternae are coated, budding structures at their rims (Figure 4, A and B, arrows) but occasionally also on their planar face (Figure 4C, arrow), which could be labeled by anti-clathrin antibodies. Clathrin-coated vesicles (Figure 4, A–C, and F, arrowheads) distinctly smaller in size (50–60 nm in diameter) than those arising at the flagellar pocket (cf. Figure 4D) were regularly found near the endosomes. We designate these vesicles class II clathrin-coated vesicles. In addition, a clathrin coat was present at the rim (Figure 4E, arrow) or along the external face of the outermost *trans*-Golgi cisterna (Figure 4F, arrows), a pattern observed only on some Golgi profiles (see unlabeled Golgi complex in Figure 4B).

Remarkably, the coated vesicles of class II budding from endosomal cisternae turned out to be depleted in VSG relative to the core of the cisternae (Figure 5, A and B). This is particularly evident in the endosomal structure shown in Figure 5A, which shows multiple endosomal buds essentially free of VSG-specific immunogold label, whereas the endosomal core is strongly positive for VSG. In principle, this pattern could be an artifact, if the antigen in the buds would be buried below the section's surface and, therefore, not accessible to antibodies and Protein A gold. Two observations argue against this possibility. First, in the very thin cryosection shown in Figure 5C, the bud was decorated by a single gold grain (demonstrating that it is accessible) but its labeling density was weak compared with the core of the cisterna. Second, the double-labeling experiments shown in Figure 5, D–F, clearly indicated that VSG was not detectable

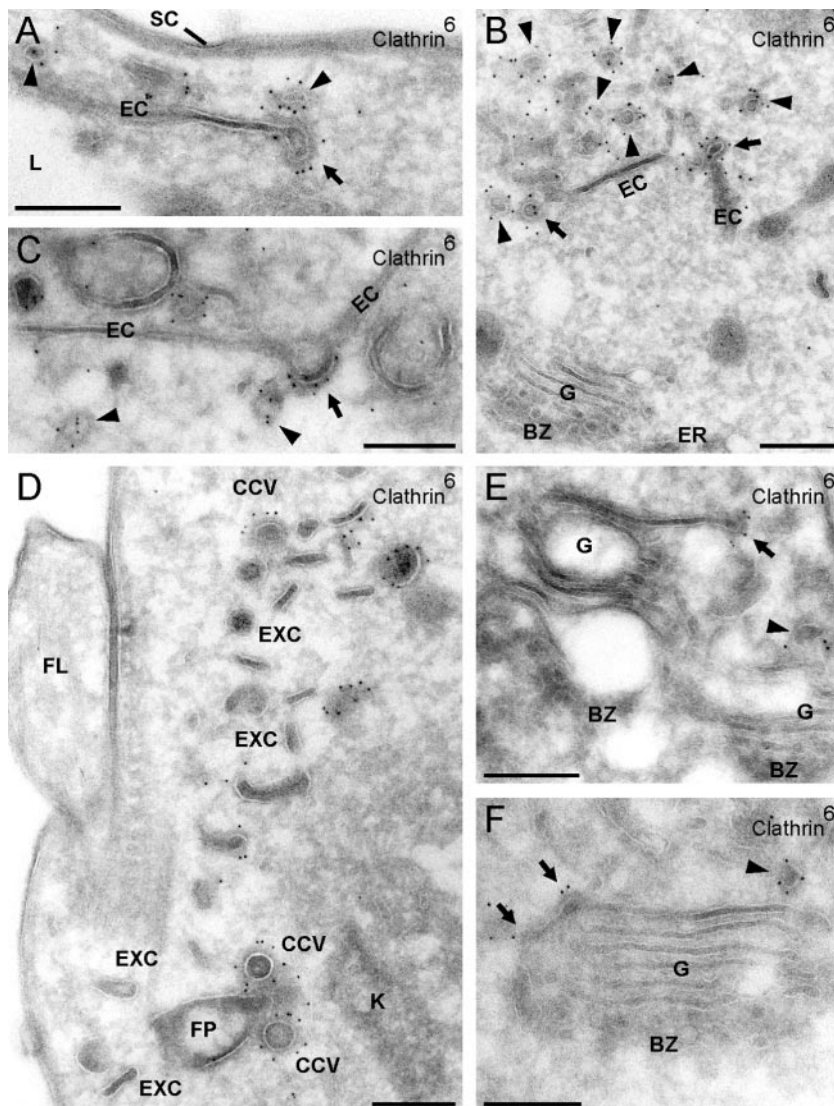


**Figure 4.** Association of clathrin with endosomal cisternae and the Golgi complex. Cryosections were labeled with anti-clathrin antibodies and PAG-6. Clathrin-mediated budding (A and B, arrows) is frequently observed at the rims of the EC, but sometimes also on planar regions (see arrow pointing at a bent cisterna in C). The pinched-off vesicles (A–C, E, and F, arrowheads) are smaller than CCVs derived from the flagellar pocket membrane (cf. D and Figure 3, B, C, and E). The EXCs (D) are not labeled. Although most Golgi profiles (see G in B) are not labeled, in some images a clathrin coat is present at the ends of (E, arrow) or along the external face of the outermost *trans*-Golgi cisterna (F, arrows). BZ, budding zone between ER and *cis*-Golgi; FL, flagellum; K, kinetoplast. Bars (A–F), 250 nm.

in the clathrin-positive buds (arrows) and vesicles (arrowheads), although the cisternal core was strongly positive. We conclude that class II vesicles budding from endosomes are depleted of VSG relative to the cisternal core structure, from which they originate.

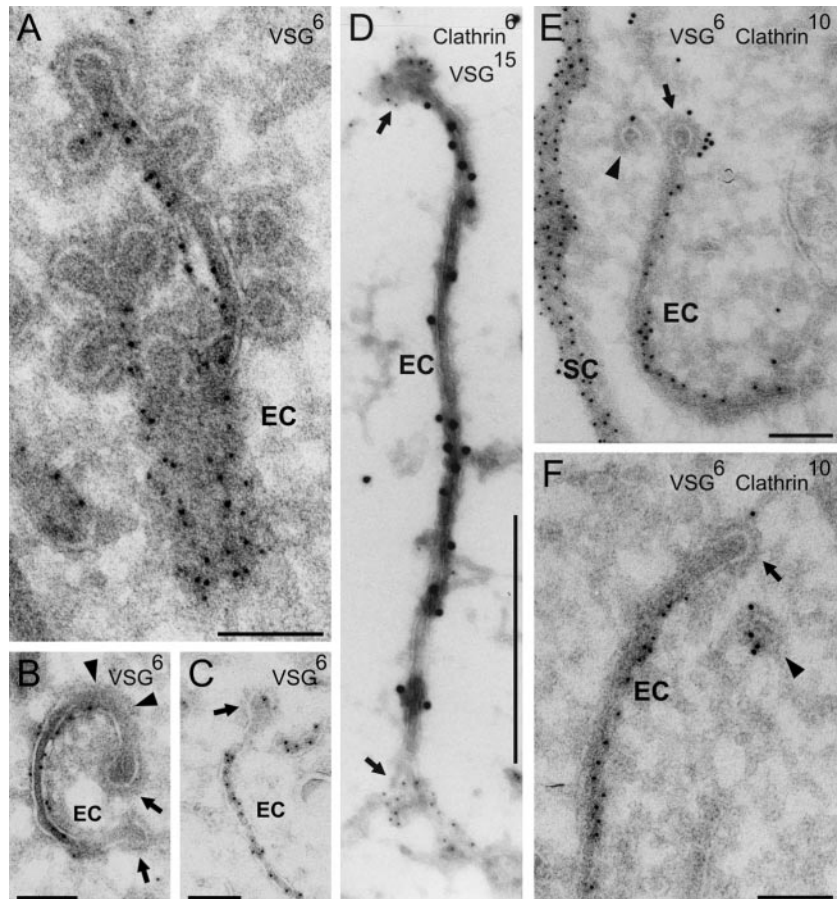
#### **VSG Is Recycled to the Flagellar Pocket by *TbRAB11*-positive Carriers**

Because VSG is rapidly taken up by endocytosis but, at the same time, is metabolically very stable, it has been suggested that >95% of the internalized protein is recycled to the cell surface (Seyfang *et al.*, 1990). This implies that VSG/membrane endocytosis is compensated by exocytosis and, in first approximation, the rate of transport must be the same in both directions. In mammalian cells, the small GTPase RAB11 is an established marker for recycling endosomes (Ullrich *et al.*, 1996; Sönnichsen *et al.*, 2000) and recently, a

homolog, *TbRAB11*, has been characterized in *T. brucei* (Jeffries *et al.*, 2001). Therefore, this marker offered the opportunity to investigate structures involved in recycling of VSG.

On the fluorescence microscopic level, anti-*TbRAB11* antibodies showed binding to well-defined, continuous subareas of the endocytic compartment (Figure 2, D–F; Jeffries *et al.*, 2001). In all cells analyzed, a distinct signal was obtained juxtaposed to the flagellar pocket membrane (Figure 2E, arrowhead). This is likely the site where recycling, VSG-containing, exocytic carriers (see below) fuse with the plasma membrane. Interestingly, a high percentage of *TbRAB11* colocalized with VSG distant from the flagellar pocket, and we have always detected *RAB11*-positive structures close to the lysosome (Figure 6, A and B). Maximum intensity and shadow projections of 3D images indicated that virtually all *RAB11*-positive structures carry VSG (Figure 2, D and F). Volume rendering showed that a significant fraction of *TbRAB11*-positive structures was embedded

**Figure 5.** Clathrin-coated vesicles budding from endosomes are deficient in VSG. Cryosections were labeled with anti-VSG antibodies and PAG-6 (A–C) or double labeled with anti-clathrin and anti-VSG antibodies and PAG-6, PAG-10, or PAG-15 as indicated (D–F). (A) An EC with numerous clathrin-coated buds has been sectioned perpendicularly in the upper part and in plane in the lower part. Whereas the lumen of the cisterna is strongly labeled for VSG, the buds are nearly VSG free. (B) The buds (arrows) as well as an adjacent region of the cisterna (arrowheads) are clathrin-coated but free of VSG. The latter region may indicate an incipient clathrin-coated bud. (C) A very thin cryosection with a single gold grain inside the terminal bud (arrow) at the rim of the cisterna. (D–F) Budding structures on cisternae marked by arrows are positive for clathrin and negative for VSG, whereas the reverse pattern is observed for their sheet-like core region. Adjacent, free clathrin-coated vesicles (E and F, arrowheads) are also free of VSG. SC, surface coat. Bars (A, B, E, and F), 125 nm; 250 nm (C); and 500 nm (D).



within the endocytic compartment (Figure 2E). Quantitative colocalization analysis disclosed that  $27.8 \pm 2.7\%$  of all endocytosed VSG colocalized with TbRAB11, whereas  $89.2 \pm 6.5\%$  of TbRAB11 colocalized with VSG ( $n = 17$ ).

On the electron microscopic level, both extended and circular profiles of the cisternae could be labeled on their cytosolic face by anti-TbRAB11 antibodies (Figure 6A, arrowheads), and a quantitative evaluation of 400 randomly selected sections showed that 51.7% of all endosomal profiles were positive for this protein. Some label was also associated with the *trans*-Golgi cisternae (Figure 6B, arrowhead). The most strongly labeled TbRAB11-positive, intracellular structures were flat, disk-shaped vesicles, which we have named EXCs. They are sausage-shaped in cross sections (Figures 6, E and F, and 7A;  $153.6 \pm 5.9$  nm in length,  $33.7 \pm 0.5$  nm in thickness) but reveal their plate-like structure when sectioned in-plane (Figure 6D, asterisk;  $150 \pm 3.8$  nm in diameter) or tangentially (Figure 7D, asterisk). Exocytic carrier vesicles were located in abundance near the flagellar pocket (Figure 6, E and F) but were also found near endosomal cisternae close to the lysosome (Figure 6A). They approach the flagellar pocket in an orientation perpendicular to the plane of the target membrane (Figure 7, A and C) and then fuse (Figure 7, B and D). Importantly, the clathrin-coated pits budding from the flagellar pocket membrane did not react with anti-TbRAB11 antibodies (Figure 7, C and D).

Together with the endocytic vesicles, exocytic carriers had the highest VSG concentration of all intracellular structures (Figure 6F) and in the steady state, they were strongly positive for surface-derived biotinylated VSG (our unpublished data). An important question was whether the VSG density (molecules/membrane area) in the exocytic carriers was as high as or even higher than on the flagellar pocket membrane/cell surface. By counting the number of gold grains per membrane length on ultrathin cryosections, we estimated that the ratio in label density between the exocytic carriers and the plasma membrane is  $\sim 0.5$  rather than  $\geq 1$ . This ratio may be an underestimate for experimental reasons. First, on cryosections (but not on plastic sections), the cell surface was labeled along the whole section thickness (confirmed by inspection of stereo images), whereas cytoplasmic structures were only labeled at the section surface. Therefore, this edge effect can result in an artificial overestimate of VSG density at the cell surface relative to that on intracellular membranes. Second, at high antigen density, the labeling efficiency is limited by electrostatic repulsion and/or steric hindrance of Protein A gold complexes (Griffiths, 1993). Thus, it is conceivable that these effects are more pronounced in the tightly opposed VSG layers of the flat exocytic carriers than on the single-layered plasma membrane, resulting in an underestimate of antigen density in the carriers.

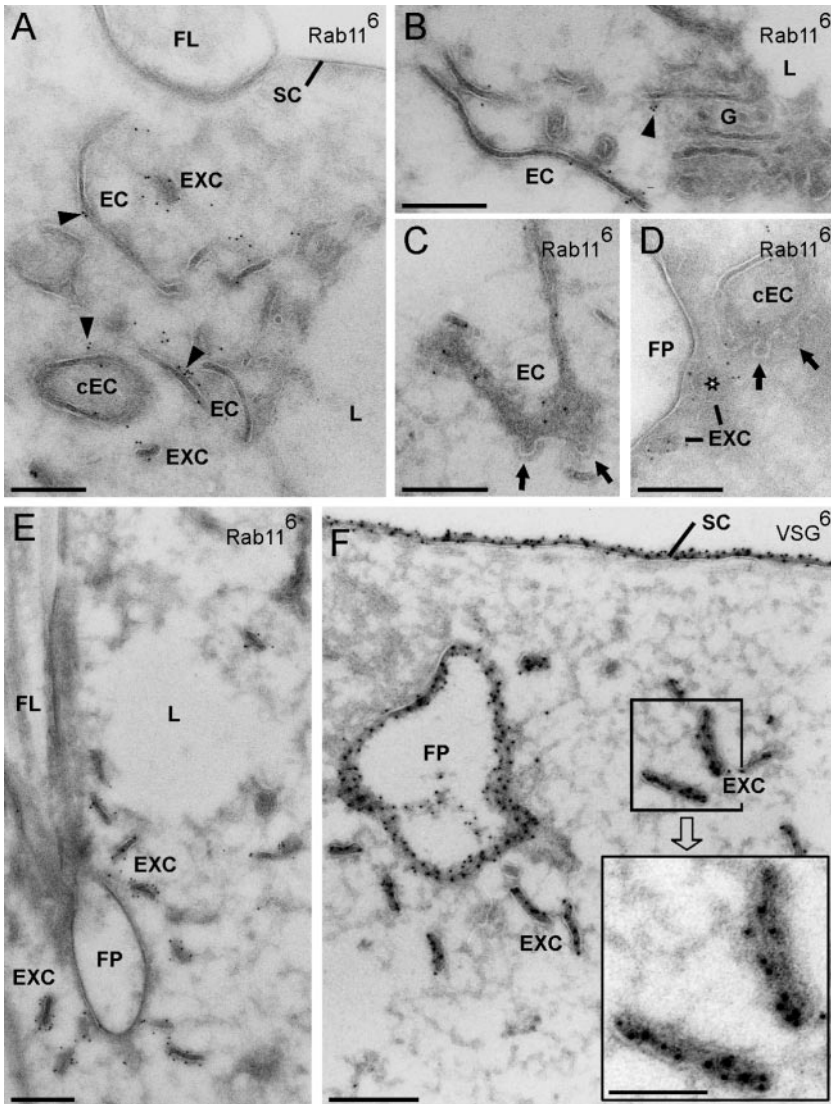


**Figure 6.** TbRAB11 marks endosomal cisternae and exocytic carrier vesicles rich in VSG. Cryosections were labeled with anti-TbRAB11 (A–E) or anti-VSG antibodies (F) and PAG-6. (A) Extended or circular profiles of endosomal cisternae (EC and cEC, respectively) near the lysosome (L). Some cisternae (arrowheads) and EXCs are labeled by anti-TbRAB11 antibodies. (B) The TbRAB11 protein is localized on the cytoplasmic side of endosomal membranes and occasionally, on cisternae of the Golgi complex (G, arrowhead). (C and D) TbRAB11-positive endosomes with several budding clathrin-coated pits (arrows). The asterisk marks an in-plane cross-sectioned EXC. (E) In contrast to the cisternae, the exocytic carrier vesicles are uniformly and strongly labeled for TbRAB11. (F) Together with the endocytic vesicles, the exocytic carriers have the highest VSG-concentration of all intracellular structures (compare the label density of the exocytic carriers [higher magnification in the inset] with that of perpendicularly sectioned regions of the VSG surface coat [SC]). Bars (A–F), 250 nm; inset (F), 125 nm.

**DISCUSSION**

***Clathrin-mediated Budding in T. brucei Occurs at the Flagellar Pocket, on Endosomes and a trans-Golgi Cisterna***

The variant surface glycoprotein enters the cells through class I clathrin-coated pits and vesicles. For several reasons, we believe that this is the dominant and most likely the only endocytic pathway in *T. brucei*. First, because the flagellar pocket membrane is limited in area (3–7% of the total cell surface; Grünfelder *et al.*, 2002) and well defined with its balloon-like shape, particularly in high-pressure-frozen cells, it is unlikely that alternative endocytic invaginations would have gone unnoticed, considering the large number of ultrastructural studies on trypanosomes performed in this and other laboratories. Second, class I clathrin-coated pits and vesicles at and near the flagellar pocket are found in abundance, and this correlates with the distinct, overlapping VSG/clathrin-containing region close to the flagellar pocket

in fluorescence microscopic images (Figure 2, A–C). Therefore, these vesicles are formed at a high frequency, consistent with the rapid rate of receptor-mediated and fluid phase endocytosis by the parasite (Coppens *et al.*, 1987). Third, if surface-biotinylated cells are allowed to endocytose for short times, intracellular VSG<sub>biotin</sub> is readily and only observed in this class of coated vesicles, strongly suggesting that VSG enters the cell solely by this pathway. The further investigation of this route, i.e., by a biochemical characterization of isolated coated vesicles (Shapiro and Webster, 1989), is likely of considerable interest considering that their composition may be unusual; *T. brucei* apparently lacks a homolog for the adaptin, AP2, the heterotetrameric complex associated with clathrin-mediated endocytosis in mammalian cells (Morgan *et al.*, 2002b).

As judged by immunofluorescence (Figure 2, A–C), most of the cellular clathrin is located at a distance from the flagellar pocket in the direction of the nucleus. The majority of this clathrin colocalizes with biotinylated VSG taken up to

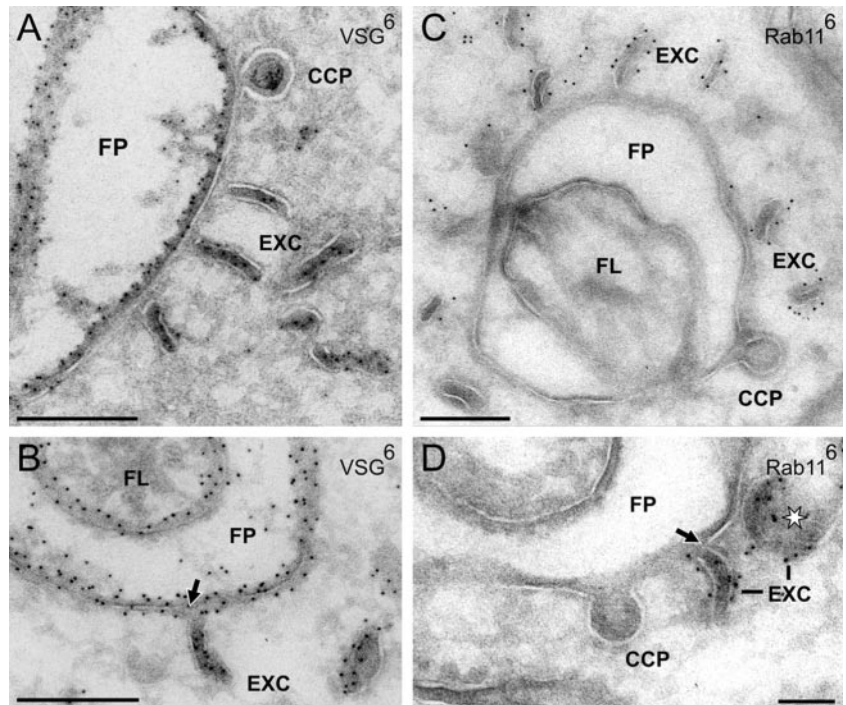


**Figure 7.** The TbRAB11-positive and VSG-rich carriers fuse with the membrane of the flagellar pocket. Cryosections were either labeled with anti-VSG (A and B) or anti-TbRAB11 antibodies (C and D) and PAG-6. The disk-like EXCs approach the FP in an orientation perpendicular to the plane of the target membrane (A and C) and then fuse (B and D). The arrows in B and D mark points of continuity between the two membranes. The endocytic CCPs in C and D do not react with anti-TbRAB11. The asterisk marks an exocytic carrier in top view. Bars, 250 nm.

the steady state by endocytosis; however, there is no overlap with VSG for approximately one-third of the clathrin. This distribution is consistent with the immunoelectron microscopic results. Cisternal endosomes positive for VSG in their core region display clathrin-coated budding structures designated class II, which are essentially free of VSG (Figures 4 and 5). Moreover, in the vicinity of the cisternae, class II clathrin-coated vesicles are found in abundance, which are also deficient in VSG and are, therefore, most likely derived from these cisternae. The target membrane for the class II coated vesicles remains unknown (compare legend to Figure 1).

In mammalian cells, abundant endosomal clathrin-coated buds and derived vesicles with a diameter of 60 nm, i.e., similar in size to those observed herein, and generally negative for the adaptor complex AP2, were described by Stoorvogel *et al.* (1996); the authors considered that these coated vesicles are involved in recycling from early endosomes to the plasma membrane or to the *trans*-Golgi network (TGN). In contrast, Futter *et al.* (1998) showed that coated buds on endosomal tubules contained a subunit characteristic for the adaptor complex AP1; these buds were proposed to be responsible for concentrating the transferrin receptor being packaged for basolateral sorting in MDCK cells. A recent study in HeLa cells by van Dam and Stoorvogel (2002) suggests that the pathway from recycling endosomes to the plasma membrane is mediated, at least in part, by endosome-derived clathrin-coated vesicles. Thus, the target membrane for these vesicles likewise remains to be defined.

There seems to be a third clathrin-dependent budding process in *T. brucei* occurring at the outermost *trans*-Golgi cisterna (Figure 4). Because tubular-vesicular structures defining the TGN in mammalian cells have not been observed in this organism, this cisterna may be the TGN equivalent

(Field *et al.*, 2000; McConville *et al.*, 2002a), and, like in mammalian cells, clathrin may be involved in the sorting of lysosomal proteins (Alexander *et al.*, 2002).

#### **RAB11-positive Carriers Mediate Transport of VSG from Endosomes to the Flagellar Pocket**

About half of all endosomal cisternae can be designated recycling endosomes because they contain the small GTPase TbRAB11. Some of these cisternae may be interconnected (Webster, 1989) and by analogy to mammalian cells (Sönichsen *et al.*, 2000), they may be organized as a mosaic of domains, which recruit different RAB proteins to subregions of the same structure. We propose that these cisternae are the source of the characteristic disk-like vesicles designated exocytic carriers, which 1) are strongly positive for TbRAB11 and VSG, 2) have a similar thickness and structural appearance as the cisternae in cross section, and 3) are generally observed in the vicinity of cisternae. Because of their abundance particularly close to the flagellar pocket, we consider these carriers as the dominant and likely the only vesicular structures that transport membrane from the endosomal compartment to the flagellar pocket. This implies that the flow of VSG/membrane entering the cell via class I clathrin-coated vesicles is balanced by a reverse flow by way of TbRAB11-positive exocytic carriers. Kinetic experiments on the rates of VSG-endocytosis and recycling support this view (unpublished data). They show that clathrin-containing structures become VSG<sub>biotin</sub>-positive before the TbRAB11-carrying structures (Figure 3E) arguing against an endocytic function of the TbRAB11-positive carrier vesicles. To balance the endocytic membrane flow via class I CCVs, the EXCs must be assumed to fuse with the flagellar pocket rather than deliver the VSG by a kiss and run mechanism.

This view is strongly supported by the phenotype of cells where clathrin-function has been abolished using the RNA interference technology. There, the size of the flagellar pocket increases dramatically, which is consistent with an inhibition of inward but unhindered outward membrane flow (Engstler, unpublished data).

### Trafficking and Sorting of VSG

The VSG at the surface coat has a purity of  $\geq 95\%$ , and the density of this protein at the surface is 50-fold higher than on the membrane of the ER. Therefore, VSG is very efficiently separated from other proteins as well as laterally concentrated. This concentration gradient is achieved in two (ER  $\rightarrow$  Golgi complex  $\rightarrow$  flagellar pocket membrane) or three steps (ER  $\rightarrow$  Golgi complex  $\rightarrow$  endosomes  $\rightarrow$  flagellar pocket membrane). If exocytosis exclusively occurs via TbRAB11-positive exocytic carriers as suggested above, then newly synthesized VSG may be routed directly or indirectly from the Golgi complex to TbRAB11-positive recycling endosomes and carriers to the flagellar pocket. VSGs endocytosed at the flagellar pocket reaches these recycling endosomes probably via TbRAB5-positive early endosomes, which seem to be preferentially located close to the nucleus rather than in the direct vicinity of the flagellar pocket (Pal *et al.*, 2002; Engstler and Grünfelder, unpublished data).

The multiple steps at which VSG is sorted and concentrated may involve both positive and negative selection mechanisms. Based on the observations presented in this article, we can only comment on two of these steps. First, we suggest that inclusion of the VSG coat in class I clathrin-coated pits and vesicles is essentially a passive process, which involves no gross changes in VSG concentration. However, without an accurate quantification in terms of molecules/membrane area, it remains possible that the VSG concentration in the vesicles (e.g., due to steric hindrance) is in fact somewhat lower than at the flagellar pocket membrane. Second, we provide a rather strong argument for sorting of VSG by default in the recycling endosomes. The class II clathrin-coated vesicles budding from VSG-positive endosomal cisternae are strongly depleted in VSG, implying that VSG is concentrated by negative selection in the cisternae (Figure 5). We previously noted (Grünfelder *et al.*, 2002) that the membrane concentration of VSG in cisternal structures increases two- to fourfold in a direction from the nucleus to the flagellar pocket and that the concentration is particularly high in circular cisternal profiles located close to the flagellar pocket. These observations are consistent with a gradual increase in the lateral VSG density as more and more membrane depleted in VSG is removed. As expected, the VSG concentration in the exocytic carriers is high and approaches the surface density, but for the technical reasons discussed above, may be underestimated relative to the cell surface.

Our observations can be compared with studies on trafficking and sorting in mammalian cells and yeast. As pointed out by Sabharanjak *et al.* (2002), nonselective uptake, i.e., without significant changes in membrane density, is the most parsimonious mechanism for GPI-anchored protein internalization by various routes in mammalian cells, given their uniform, diffuse distribution at the cell surface. There is now agreement that GPI-anchored proteins are not enriched in clathrin-coated pits/vesicles or in caveoli relative to the

plasma membrane (reviewed in Chatterjee and Mayor, 2001). However, a recently described cdc42-regulated, clathrin- and caveolin-independent pinocytic pathway in COS and Chinese hamster ovary cells has been suggested to recruit GPI-linked proteins from the cell surface into a specific peripheral tubular-vesicular, early endosomal compartment, where they seem to be (secondarily?) enriched. Thereafter, they are delivered to pericentriolar recycling endosomes, where they are retarded by a sphingolipid- and cholesterol-dependent mechanism relative to bulk membrane constituent before being routed back to the plasma membrane by so far undefined carriers (Mayor *et al.*, 1998; Chatterjee *et al.*, 2001; Sabharanjak *et al.*, 2002). These authors invoke sphingolipid- and cholesterol-rich lipid microdomains to explain both the selective uptake of GPI-anchored proteins into the specific endocytic compartment as well as their transient retention in recycling endosomes. In a recent article, Fivaz *et al.* (2002) concluded that the differential sorting and fate of GPI-anchored proteins in endosomes of baby hamster kidney and Chinese hamster ovary cells depends on their residence time in lipid microdomains. In the Golgi/trans-Golgi network of polarized Madin-Darby canine kidney and nonpolarized PtK<sub>2</sub> cells, lateral segregation and subsequent incorporation into distinct transport carriers has been shown for a trans-membrane and a GPI-anchored cargo (Keller *et al.*, 2001). Finally, sorting of GPI-anchored proteins into defined carriers has been demonstrated upon exit of the ER in yeast (Muñiz *et al.*, 2001). Together, these studies suggest that sorting of GPI-linked proteins can occur in endosomes as well as at several stages in the biosynthetic pathway.

### Is Cellular Sorting the Key to GPI-Anchor Function?

The question why there is a glycolipid anchor as a mode for attaching proteins to membranes has puzzled investigators for two decades (Ferguson, 1999; Chatterjee and Mayor, 2001). The "raft" hypothesis (Simons and Ikonen, 1997) suggests a function in cellular sorting by postulating that GPI-anchored proteins have a tendency to associate with highly dynamic liquid-ordered lipid domains formed in the liquid-disordered lipid bulk phase of a membrane. As summarized in a recent article by Anderson and Jacobson (2002), no consensus about the size, shape, and location of these domains at the surface of mammalian cells has emerged. In its second part, the hypothesis proposes that such domains are specifically incorporated into transport carriers formed, for example, at the trans-Golgi network for selective delivery of GPI-anchored proteins to the cell surface. The difficulty with this proposition is that it implies a sorting mechanism, which specifically identifies GPI-linked proteins and/or lipid-ordered domains from the opposite, cytosolic face of a membrane and ensures their preferential inclusion into vesicular carriers. Based on the observations on endosomal sorting reported in this study, we would like to suggest an alternative scenario. GPI-anchored proteins can be specifically excluded from structures budding from a given intracellular membrane, thereby being sorted and laterally concentrated by negative selection. This may still involve association with fluid-ordered lipid domains; however, these domains would not be included into budding structures. The excluded regions enriched in the GPI-anchored and, likely, other components such as sphingolipids or mul-

tipass trans-membrane proteins such as transporters would then give rise to carriers such as the exocytic vesicles described in this study. In conclusion, the essence of the glycolipid anchor function would be that it is neglected by coats, which are involved in positive sorting of trans-membrane proteins. In trypanosomes, multiple negative sorting steps may operate to achieve the high VSG concentration at the cell surface, which is vital for survival in the mammalian vascular system providing a highly dynamic shield against antibodies toward buried invariant surface proteins as well as against attack by complement.

## ACKNOWLEDGMENTS

We thank Sabine Geier for expert technical assistance and Drs. Michael Boshart (Munich, Germany), Anne Spang, and Suzanne Gokool (both from Tübingen, Germany) for reading the manuscript and helpful discussions. M.E. thanks Michael Boshart for continuous support in the laboratory. P.O. acknowledges funding by the Fond der Chemischen Industrie (Frankfurt, Germany), and M.B. by the Deutsche Forschungsgemeinschaft. G.W.M. and M.C.F. are supported by the Wellcome Trust (London, United Kingdom).

## REFERENCES

- Alexander, D.L., Schwartz, K.L., Balber, A.E., and Bangs, J.D. (2002). Developmentally regulated trafficking of the lysosomal membrane protein p67 in *Trypanosoma brucei*. *J. Cell Sci.* *115*, 32543–3263.
- Anderson, R.G.W., and Jacobson, K. (2002). A role for lipid shells in targeting proteins to caveolae, rafts, and other lipid domains. *Science* *296*, 1821–1825.
- Bamezai, A., Goldmacher, V.S., and Rock, K.L. (1992). Internalization of glycosyl-phosphatidylinositol (GPI)-anchored lymphocyte proteins. II. GPI-anchored and transmembrane molecules internalize through distinct pathways. *Eur. J. Immunol.* *22*, 15–21.
- Bretscher, M.S., Thomson, J.N., and Pearse, B.M.F. (1980). Coated pits act as molecular filters. *Proc. Natl. Acad. Sci. USA* *77*, 4156–4159.
- Brown, D.A., and London, E. (2000). Structure and function of sphingolipid- and cholesterol-rich membrane rafts. *J. Biol. Chem.* *275*, 17221–17224.
- Chatterjee, S., and Mayor, S. (2001). The GPI-anchor and protein sorting. *Cell Mol. Life Sci.* *58*, 1969–1987.
- Chatterjee, S., Smith, E.R., Hanada, K., Stevens, V.L., and Mayor, S. (2001). GPI anchoring leads to sphingolipid-dependent retention of endocytosed proteins in the recycling endosomal compartment. *EMBO J.* *20*, 1583–1592.
- Coppens, I., Opperdoes, F.R., Courtoy, P.J., and Baudhuin, P.B. (1987). Receptor-mediated endocytosis in the bloodstream form of *Trypanosoma brucei*. *J. Protozool.* *34*, 465–473.
- Cross, G.A.M. (1996). Antigen variation in trypanosomes: secrets surface slowly. *Bioessays* *18*, 283–291.
- Ferguson, M.A.J. (1999). The structure, biosynthesis and functions of glycosylphosphatidylinositol anchors, and the contributions of trypanosome research. *J. Cell Sci.* *112*, 2799–2809.
- Field, H., Sherwin, T., Smith, A.C., Gull, K., and Field, M.C. (2000). Cell-cycle and developmental regulation of TbRAB31 localization, a GTP-locked Rab protein from *Trypanosoma brucei*. *Mol. Biochem. Parasitol.* *106*, 21–35.
- Fivaz, M., Vibois, F., Thrunheer, S., Pasquali, C., Ambrami, L., Bickel, P.E., Parton, R.G., and van der Goot, F.G. (2002). Differential sorting and fate of endocytosed GPI-anchored proteins. *EMBO J.* *21*, 3989–4000.
- Futter, C.E., Gibson, A., Allchin, E.H., Maxwell, S., Ruddock, L.J., Odorizzi, G., Domingo, D., Trownbridge, I.S., and Hopkins, C.R. (1998). In polarized MDCK cells basolateral vesicles arise from clathrin- $\gamma$ -adaptin-coated domains on endosomal tubules. *J. Cell Biol.* *141*, 611–623.
- Griffiths, G. (1993). *Fine Structure Immunocytochemistry*. Heidelberg: Springer Verlag.
- Grünfelder, C.G., Engstler, M., Weise, F., Schwarz, H., Stierhof, Y.-D., Boshart, M., and Overath, P. (2002). Accumulation of a GPI-anchored protein at the cell surface requires sorting at multiple intracellular levels. *Traffic* *3*, 547–559.
- Harder, T., Scheiffele, P., Verkade, P., and Simons, K. (1998). Lipid domain structure of the plasma membrane revealed by patching of membrane components. *J. Cell Biol.* *141*, 929–942.
- Jeffries, T.R., Morgan, G.W., and Field, M.C. (2001). A developmentally regulated Rab11 homologue in *Trypanosoma brucei* is involved in recycling processes. *J. Cell Sci.* *114*, 2617–2626.
- Keller, G.A., Siegel, M.W., and Caras, I.W. (1992). Endocytosis of glycosphospholipid-anchored and transmembrane forms of CD4 by different endocytic pathways. *EMBO J.* *11*, 863–874.
- Keller, P., Toomre, D., Diaz, E., White, J., and Simons, K. (2001). Multicolour imaging of post-Golgi sorting and trafficking in live cells. *Nat. Cell Biol.* *3*, 140–149.
- Killish, K., Steinlein, P., Römisch, K., Hollingshead, R., Beug, H., and Griffiths, G. (1992). Characterization of early and late endocytic compartments of the transferrin cycle. *J. Cell Sci.* *103*, 211–232.
- Kirchhausen, T. (2000). Three ways to make a vesicle. *Nat. Rev. Mol. Cell Biol.* *1*, 187–198.
- Landfear, S., and Ignatushchenko, M. (2001). The flagellum and flagellar pocket of trypanosomatids. *Mol. Biochem. Parasitol.* *115*, 1–17.
- Langreth, S.G., and Balber, A.E. (1975). Protein uptake and digestion in bloodstream and culture forms of *Trypanosoma brucei*. *J. Protozool.* *22*, 40–53.
- Mayor, S., Sabharanjak, S., and Maxfield, F.R. (1998). Cholesterol-dependent retention of GPI-anchored proteins in endosomes. *EMBO J.* *17*, 4626–4638.
- McConville, M.J., and Ferguson, M.A.J. (1993). The structure, biosynthesis and function of glycosylated phosphatidylinositols in the parasitic protozoa and higher eukaryotes. *Biochem. J.* *294*, 305–324.
- McConville, M.J., Ilgoutz, S.C., Teasdale, R.D., Foth, B.J., Matthews, A., Mullin, K.A., and Gleeson, P.A. (2002a). Targeting of the GRIP domain to the *trans*-Golgi network is conserved from protists to animals. *Eur. J. Cell Biol.* *81*, 485–495.
- McConville, M.J., Mullin, K.A., Ilgoutz, S.C., and Teasdale, R.D. (2002b). Secretory pathway of trypanosomatid parasites. *Microbiol. Mol. Biol. Rev.* *66*, 122–154.
- Morgan, G.W., Allen, C.L., Jeffries, T.R., Hollinshead, M., and Field, M.C. (2001). Developmental and morphological regulation of clathrin-mediated endocytosis in *Trypanosoma brucei*. *J. Cell Sci.* *114*, 2605–2615.
- Morgan, G.W., Hall, B.S., Denny, P.W., Field, M.C., and Carrington, M. (2002a). The kinetoplast endocytic apparatus. Part I: a dynamic system for nutrition and evasion of host defences. *Trends Parasitol.* *18*, 491–496.
- Morgan, G.W., Hall, B.S., Denny, P.W., Field, M.C., and Carrington, M. (2002b). The endocytic apparatus of the kinetoplastida. Part II: machinery and components of the system. *Trends Parasitol.* *18*, 540–546.

- Muñiz, M., Mosomme, P., and Riezman, H. (2001). Protein sorting upon exit from the endoplasmic reticulum. *Cell* 104, 313–320.
- Overath, P., Chaudhri, M., Steverding, D., and Ziegelbauer, K. (1994). Invariant surface proteins in bloodstream forms of *Trypanosoma brucei*. *Parasitol. Today* 2, 53–58.
- Overath, P., Stierhof, Y.-D., and Wiese, M. (1997). Endocytosis and secretion in trypanosomatid parasites - tumultuous traffic in a pocket. *Trends Cell Biol.* 7, 27–33.
- Pal, A., Hall, B.S., Nesbeth, D.N., Field, H.I., and Field, M.C. (2002). Differential endocytic functions of *Trypanosoma brucei* Rab5 isoforms reveal a glycosylphosphatidylinositol-specific endosomal pathway. *J. Biol. Chem.* 277, 9529–9539.
- Sabharanjak, S., Sharma, P., Parton, R.G., and Mayor, S. (2002). GPI-anchored are delivered to recycling endosomes via a distinct cdc42-regulated, clathrin-independent pinocytic pathway. *Dev. Cell* 2, 411–423.
- Seyfang, A.D., Mecke, D., and Duscenko, M. (1990). Degradation, recycling and shedding of *Trypanosoma brucei* variant surface glycoprotein. *J. Protozool.* 37, 546–552.
- Shapiro, S.Z., and Webster, P. (1989). Coated vesicles from the protozoan parasite *Trypanosoma brucei*: purification and characterization. *J. Protozool.* 36, 344–349.
- Simons, K., and Ikonen, E. (1997). Functional rafts in cell membranes. *Nature* 387, 569–572.
- Simons, K., and van Meer, G. (1988). Lipid sorting in epithelial cells. *Biochemistry* 27, 6197–6202.
- Sönnichsen, B., de Renzis, S., Nielsen, E., Rietdorf, J., and Zerial, M. (2000). Distinct membrane domains on endosomes in the recycling pathway visualized by multicolour imaging of Rab4, Rab5 and Rab11. *J. Cell Biol.* 149, 901–913.
- Stierhof, Y.-D., Bates, P.A., Jacobson, R.L., Rogers, M.E., Schlein, Y., Handman, E., and Ilg, T. (1999). Filamentous proteophosphoglycan secreted by *Leishmania* promastigotes forms gel-like three-dimensional networks that obstruct the digestive tract of infected sandfly vectors. *Eur. J. Cell Biol.* 78, 675–689.
- Stoorvogel, W., Oorschot, V., and Geuze, H.J. (1996). A novel class of clathrin-coated vesicles budding from endosomes. *J. Cell Biol.* 132, 21–33.
- Ullrich, O., Reinsch, S., Urbe, S., Zerial, M., and Parton, R.G. (1996). Rab11 regulates recycling through a perinuclear recycling endosome. *J. Cell Biol.* 13, 913–924.
- van Dam, E.M., and Stoorvogel, W. (2002). Dynamin-dependent transferring receptor recycling by endosome-derived clathrin-coated vesicles. *Mol. Biol. Cell* 13, 169–182.
- Vickermann, K. (1969). On the surface coat and cellular adhesion in trypanosomes. *J. Cell Sci.* 5, 163–193.
- Webster, P. (1989). Endocytosis by African trypanosomes. I. Three-dimensional structure of the endocytic organelles in *Trypanosoma brucei* and *Trypanosoma congolense*. *Eur. J. Cell Biol.* 49, 295–302.
- Webster, P., and Grab, D. (1988). Intracellular colocalization of variant surface glycoprotein and transferrin-gold in *Trypanosoma brucei*. *J. Cell Biol.* 106, 279–288.
- Webster, P., and Shapiro, S.Z. (1990). *Trypanosoma brucei*: a membrane-associated protein in coated endocytic vesicles. *Exp. Parasitol.* 70, 154–163.
- Weise, F., Stierhof, Y.-D., Kühn, C., Wiese, M., and Overath, P. (2000). Distribution of GPI-anchored proteins in the protozoan parasite *Leishmania*, based on an improved ultrastructural description using high-pressure frozen cells. *J. Cell Sci.* 113, 4587–4603.